Chapter 3

Stabilizing Pickering emulsion by brush-modified Janus Particles

3.1 Introduction

The emulsion is a mixture of two or more liquids that do not usually mix, with one forming tiny droplets dispersed within the other. Emulsions are used in various industries, such as cosmetics, medicine, and food [154–158]. Many products, including food, vitamins, cosmetics, personal care items, and agrochemicals, use oil in water emulsions as important components [159–161]. The main components of this type of colloidal dispersion [162] are tiny oil droplets scattered throughout an aqueous phase. Emulsions are unstable and tend to degrade over time due to processes such as coalescence, particle coalescence, gravity separation, flocculation, and phase separation [161,163,164]. However, an emulsion stabilized by solid amphiphilic particles rather than surfactant molecules is called a Pickering emulsion. These particles act as emulsifiers and have both hydrophilic and hydrophobic characteristics. They adsorb at the interface of immiscible liquids, reducing interfacial tension and preventing droplet coalescence, effectively stabilizing the emulsion. Various emulsifiers and texture modifiers are used to ensure long-term stability [162]. The type of emulsifier employed affects the ease of

Pickering emulsion formation, the functional characteristics of the finished product, and its ability to stabilize Pickering emulsions. Therefore, the most important decision is to select an appropriate emulsifier when formulating Pickering emulsion-based products. Amphiphilic compounds, such as small molecule surfactants, phospholipids, proteins, polysaccharides, and other surface-active polymers, are commonly used as emulsifiers due to their dual hydrophilic and hydrophobic nature [165,166].

The formation of thermodyanmical stable Pickering emulsions has been observed with amphiphilic colloidal particles, specifically Janus particles (JPs), which have two sides with different properties. JPs have a strong tendency to loacalize at interfaces due to their distinct affinities and polarities on each side [167]. Research studies have aimed to understand how JPs self-assemble in water and respond to external forces such as magnetic and electric fields [167–170]. These investigations have revealed that amphiphilicity of JPs leads to unique colloidal phenomena, including field-driven assembly, emulsion stabilization, and drug delivery, which have both theoretical and practical significance [168,169,171–173]. Theoretical calculations and simulations have focused on JPs at fluid-fluid interfaces, explaining the detachment energy of JPs from these interfaces [174–177]. Studies have also investigated the interfacial phenomena of JPs at macroscopic scales, such as in emulsions [172,173,178,179].

Ifra and her colleagues recently used the electrodynamic co-jetting technique to create different shapes of modified MPs, including spherical ones [40,73,123,124]. These particles are made by combining the polylactide (PLA) and poly[methylmethacrylate-co-2-(2-bromopropionyloxy) ethyl methacrylate] (poly(MMA-co-BEMA)) in 3 : 1 ratio. The MP's surfaces are modified by synthesizing poly(DEMA) brushes using a grafting approach on initiator (BEMA molecule) embedded surfaces through ATRP process [40,73,123]. This process is done with DMAEMA monomer in water at $pH \sim 7$. By changing the polymerization time and and polymer brush grafting density (which refers to the number of grafted polymer chains per unit surface area), the length of polymer brushes is varied to control the surface modification. These brush-

modified MPs have various applications. The study mainly focuses on modifying the surface of spherical MPs with polymer brushes. After fabrication, half of the spherical MP becomes hydrophobic, while the other half becomes hydrophilic through ATRP brushes [1,34,40]. These brush-modified amphiphilic MPs are then used to stabilize oil emulsion in water [180–183].

In this study, we are investigating the formation of oil-in-water emulsions using brush-modified JPs as emulsifiers and stabilizers [184,185]. We are treating the entire system as an off-critical ternary fluid, with the solvent (water), oil, and JPs denoted as S, O, and C [186], respectively, undergoing phase separation (PS) [10]. The kinetics of phase separation in binary/ternary fluid mixtures are of significant interest from both fundamental and practical perspectives [9,99,187]. Numerous experimental [188,189], theoretical [9,10], and simulation [102,190,191] studies have been conducted to understand the fundamental mechanisms behind this well-known scaling phenomenon of phase separation and cluster formation [9,10]. The key parameters that characterize the morphology and its growth are the correlation function and the characteristic length scale (i.e., average domain size). The domain size follows a power-law dependence over time: $R(t) \sim t^{\phi}$, where ϕ represents the growth exponent [9]. The generally accepted values of ϕ for a typical phase-separating $3d$ system (e.g., pure oil and water mixture) are as follows: $\phi = 1/3$ (diffusive regime), 1 (viscous hydrodynamic regime), and $2/3$ (inertial hydrodynamic regime [9,10,12,192]. Our analysis focuses on the behavior of the length scale and growth exponent to evaluate the stability of the formed Pickering emulsion. Any significant decrease in ϕ, particularly when JPs are introduced into the oil and water mixture, indicates emulsion stabilization. Moreover, prolonged saturation in the length scale indicates complete pinning of the domain growth process, indicating a thoroughly stable emulsion. Achieving this state is challenging, as oil clusters may eventually merge into one large cluster over extended waiting periods, similar to the behavior observed in pure oil-water mixture segregation.

This research work presents simulation studies using DPD technique [22,23,28] to investigate the emulsification of oil in water [180–183,193] and the corresponding physical

phenomena at the mesoscale. These findings are further validated and supported by experimental results. DPD is a robust technique for simulating polymer solutions [146], polymer melts/blends [29], and gels [71] while preserving the hydrodynamic characteristics of the system. This method has been widely used to model free-radical polymerization and examine how the shape and size of complex soft materials [34–37,48,71] affect their behavior. In this study, we used a method to modify spherical MPs through surface-initiated ATRP to prepare JPs. We then examined their impact on oil-in-water emulsion. The work is organized into sections outlining the computational model and parameters, presentation of results, and conclusion. We will not be discussing the experimental part here.

3.2 Simulation methodology

3.2.1 DPD simulation

We have used the DPD simulation technique [23,27,194] and the description of this technique and other parameters which have used are give in chapter 1's section 1.4. The interaction between the particles are given in Table 3.1. The interaction for compatible beads is $a_{ii} = 25$ [150] and for incompatible beads is $a_{ij} = 60$ [37].

Table 3.1: The interaction parameter a_{ij} used in the simulation for different DPD beads.

a_{ij}	S	MP	i	M	B	O
$Solvent(S)$	25	60	30	25	27	60
$Microparticle(MP)$		30	30	40	40	25
$Initiator(i)$			30	30	30	45
$Monomer(M)$				25	25	60
$Brush(B)$					27	60
$Oil(O)$						25

The Polymer chains are modeled by the bead spring model [43,45] where beads are connected by the harmonic bond potential. The description of this model is given in chapter

1st's section 1.4.2. The formation of longer polymer chains may lead to bond crossing. To address this issue, the modified segmental repulsive potential (mSRP) [29,195,196] or FENE potential [45,102] can be utilized. However, integrating these potentials during the ATRP process is challenging. Our research focuses on polymer brushes tethered to MP surfaces. These brushes repel each other due to electrostatic and hydrophobic interactions with both surfaces, while also exhibiting hydrophilic behavior with the solvent. We will delve into this topic further shortly. As a result, the polymer brushes effectively disperse in the solvent, preventing their aggregation and reducing the likelihood of bond crossing with intermolecular and intramolecular polymer brushes.

3.2.2 Morphology characterization function and the characteristic length scale

The description of the characterization function and the characteristic length scale are given in the section 1.9.

An important function for understanding the evolution morphology of oil into the sea of solvent is the two-point equal-time spatial correlation function $C(r,t)$ [10,192]. It is given by:

$$C(\vec{r},t) = \langle \eta(\vec{r}_1,t)\eta(\vec{r}_2,t)\rangle - \langle \eta(\vec{r}_1,t)\rangle\langle \eta(\vec{r}_2,t)\rangle$$

where $\vec{r} = \vec{r}_1 - \vec{r}_2$, $\eta(\vec{r}_1,t)$ and $\eta(\vec{r}_2,t)$ are the order parameter at two discrete sites ($\vec{r}_1$ and $\vec{r}_2$) at a time t [9,10]. The angular bracket denotes the ensemble averaging over five independent runs. The order parameter $\eta(\vec{r},t)$ is defined as the local difference in concentration between different beads located on discrete lattice sites at time t. To calculate $\eta(\vec{r},t)$, we divide the simulation box into non-overlapping unit-sized boxes and count the number of solvents (water), oil, and other beads (designated as C-type) within each box, denoted as $\eta_s(\vec{r},t)$, $\eta_o(\vec{r},t)$, and $\eta_C(\vec{r},t)$. Depending on whether the number of beads of a specific type greatly exceeds the

others, we assign $\eta(\vec{r},t)$ a value of $1,-1$, or 0, respectively. In cases where any two out of the three bead numbers within a unit box are equal, but significantly higher than the third number (for example, $\eta_s(\vec{r},t) = \eta_o(\vec{r},t) > \eta_C(\vec{r},t)$), we assign the corresponding $\eta(\vec{r},t)$ with equal probability. A similar method is used for other similar situations [102,191].

A well-known aspect of phase separation kinetics is dynamic scaling in the correlation function [9].

$$C(r,t) = f(r/R(t))$$

$f(x)$ is the scaling function. The length scale $R(t)$ is computed from the correlation function as the distance it decays to zero or any fraction of its maximum value, $C(0,t) = 1$. We find that the decay of $C(r,t)$ at 0.2 provides a good measure of $R(t)$. However, several other definitions yield a similar $R(t)$ within the scaling regime, differing only by constant multiplicative factors. The average domain size often grows following a power-law relation: $R(t) \to t^{\phi}$ [29].

3.2.3 Constituting microparticle

In our simulation work, we model spherical MPs as rigid bodies. This means that we calculate all forces and torques acting on these MPs as the sum of the forces and torques on their individual beads. In experimental work, we create the MPs using PLA blended with poly (MMA-co-BEMA) on one-half of the MP surface. The poly (BEMA) compound initiates the ATRP process, which modifies the MP surfaces with polymer brushes using DMAEMA monomers available in the solution.

In our research, we simulate three different sizes of MPs. Each MP is made up of DPD beads (n_{MP}) arranged in three layers on the vertices of a geodesic grid. This grid is formed by dividing an icosahedron concentric bead [48]. We maintained the same fraction of DPD beads $\sim n_{MP}/3$ in each layer. In the system with a total of $N_{MP} = 20$MPs, the inner and outermost radius are set to $R_{in} = 1.2r_c$ and $R_o = 2.0r_c$ respectively. Each MP consists of $n_{MP} = 1086$ DPD beads. Thus, the total number of MP beads in the system is $N_{MP} \times n_{MP} = 21720$ ($\phi_{MP} = 5.7 \times 10^{-2}$).

Similar details for other sizes of MPs are provided in Table 3.2. The fraction ϕ_{MP} is computed for all DPD beads in the system. We ensured that the density of beads in MPs is sufficiently high ($\rho_m \gg 3$) in each layer to prevent the penetration of polymer brushes and other beads into it.

Table 3.2: Details of the number of beads constituting the MPs of various sizes.

N_{MP}	n_{MP}	Total MP beads	ϕ_{MP}	$R_{in}(r_c)$	$R_o(r_c)$
20	1086	21720	5.7×10^{-2}	1.2	2.0
40	486	19440	5.2×10^{-2}	0.9	1.5
80	276	22080	5.8×10^{-2}	0.5	1.0

In our experimental studies [40,73,123,124], some poly(BEMA) molecules on the MP surface act as initiators. Similarly, in our simulations, we randomly select a fraction of DPD beads N_i on half of an MP's top surface to act as initiators for the ATRP process. We analyze our results for three different sets of initiator concentrations $c_i = 1\%, 2.5\%$, and 5% of n_{MP} for each MP, corresponding to $N_i = 10, 25$, and 50 initiators per MP for the case of 20 MPs in the system. The corresponding volume fractions of the initiators are $\phi_i = 5.33 \times 10^{-4}, 1.33 \times 10^{-3}$, and 2.66×10^{-3}, respectively. Furthermore, while keeping the initiator concentration fixed at $c_i = 5\% n_{MP}$ and the total fraction of MP beads constant, we compare emulsion stability results of 20 JPs with 40 and 80 JPs.

3.2.4 Brush modification of microparticles

We use a DPD simulation technique for controlled radical polymerization (CRP) in living systems [35]. The ATRP is carried out by a series of appropriate elemental reactions to modify the initiator-embedded surfaces of MPs. This simulation approach is supported by previous experimental data [68,69] similar to earlier CRP models. These models used coarse-grained MC and MD simulations [68–70] to consider polymer geometry and the spatial distribution of active radical groups [34–36,71]. However, the spatial distribution and long-range diffusion

of active radical groups within macromolecules are significantly restricted by topological constraints and reactions between macromolecules, leading to the formation of larger clusters [68–70]. We are also using the same methodology to create the first simulation model for iniferter-based photo-controlled radical polymerization (photo-CRP) within polymer networks [34–36,71]. This model explores the relative effects of photo-initiation due to bond breaking, propagation reactions involving monomers and crosslinkers, and termination reactions in forming nanocomposite gels [37] and self-healing gels [36,38].

The current ATRP simulation process involves initiator and monomer beads and focuses on two primary reactions: initiation and monomer propagation. To grow the polymer brushes, we selected a monomer volume fraction of $\phi_M = 2.5 \times 10^{-1} (NM = 93,750)$ in the system. Importantly, we assume all initiators are active at the start of the simulation, represented by glowing pink beads in the schematic Fig. 3.1. The ATRP process begins with the random selection of initiators on the MP surface. The description of the ATRP process to modify the MPs is given in section 1.4.2.

The monomer and polymer-brush beads show the hydrophilic characteristics in water (solvent beads). As a result, we have set their mutual interaction as $a_{MS} = 25$ and $a_{BS} = 27$. Similarly, the compatible interaction between monomer and brush beads is defined as $a_{MB} = 25$. Our experimental observations show that poly(DMAEMA) brushes and MP surfaces carry a positive charge in the solvent at $pH \sim 7$ [40]. Consequently, the brushes and MPs disperse effectively in the solvent due to electrostatic repulsion, preventing their aggregation. It is important to note that including electrostatic interactions in the DPD framework [146–148] is computationally expensive when dealing with large systems [39], even with modern parallel Poisson simulators [39,148]. Therefore, incorporating charge distribution directly into the DPD simulation approach is uncommon [39,149–151]. We phenomenologically prevent their aggregation by considering effective DPD interaction parameters between brush-brush, brush-MP, and MP-MP beads as $a_{BB} = 27$, $a_{BMp} = 40$, and $a_{MpMp} = 30$. While explicit modeling of

long-range electrostatic interactions is expected to further improve brush-modified JP dispersion in a solvent, it does not impact the conclusions of this study.

The oil bead is modeled similarly to the solvent bead, with a mutual interaction parameter set at $a_{OO} = 25$. To address the immiscibility between oil and water beads, we introduce $a_{SO} = 60$. Typically, oil exhibits chemical compatibility with the MP surface ($a_{OMp} = 25$). Fig. 3.1 illustrates the hydrophobic surface of the MP (e.g., PLA surface in the experiment), which is divided into two halves - green and red. This is done only to distinguish between the initiator-free (S_1) and initiator-embedded (e.g., poly (BEMA) in the experiment) (S_2) surfaces. As a result, both S_1 and S_2 surfaces are compatible with the oil beads. Furthermore, to account for the incompatibility of oil with the initiator, brush, and monomer beads, we set the interaction strengths $a_{Oi} = 45$, $a_{OB} = a_{OM} = 60$, respectively. Our work involves emulsions of oil beads at two distinct volume fractions, $\phi_O = 5.0 \times 10^{-2}$ and 1.0×10^{-1}. The corresponding numbers of DPD beads are $N_O = 1.875 \times 10^4$ and 3.75×10^4, respectively.

In this study, we used a simulation box with dimensions of $50r_c \times 50r_c \times 50r_c$ and a fixed number density of $\rho = 3$. The box contains $N = 3.75 \times 10^5$ beads, and we applied periodic boundary conditions in all three directions. To initiate the DPD simulation, we first dispersed MPs in the simulation box, and then distributed monomer and solvent beads randomly within the same box. The system was then allowed to equilibrate for a duration of $t_{eq} = 5.0 \times 10^4$ before the polymerization reaction began. The polymer brush was initially grown for a suitable duration (t_{bg}) to yield the polymer brush fabricated MPs, termed JPs. Subsequently, oil beads were introduced randomly into the simulation box. The entire system was equilibrated again for $t_{eq} = 5.0 \times 10^4$ at a high temperature, $T = 5$. Furthermore, we monitored the temporal evolution of the emulsification process at $T = 1$.

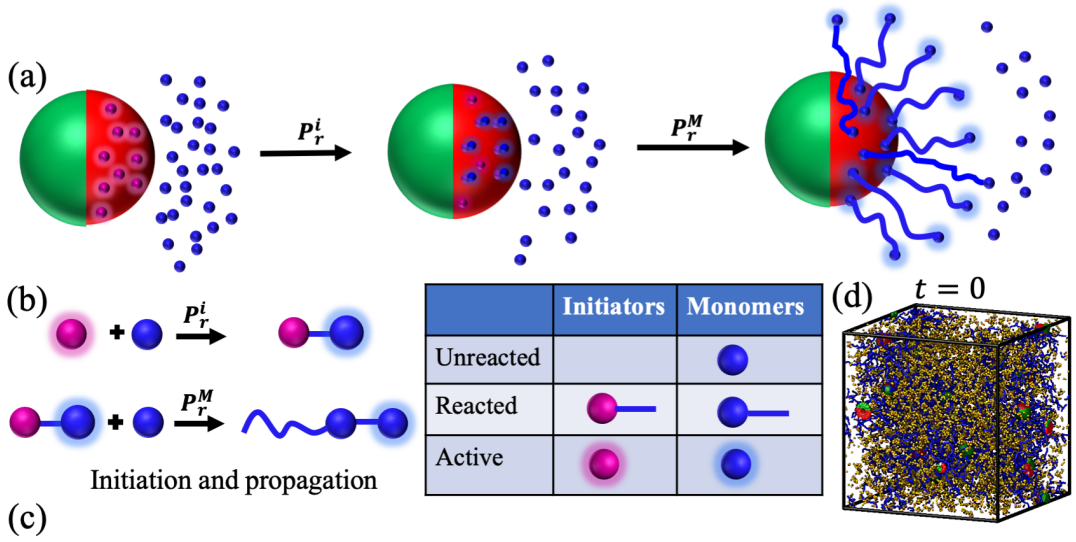

(c)

Bead type	Color	Bead/surface type	Color
Solvent	No color	Hydrophobic (S_1)	Green
Oil	Yellow	Hydrophobic (S_2)	Red

Fig. 3.1: (a) The diagram highlights the initiation and propagation reactions and key phases in ATRP reactions for brush growth. (b) Pink and blue glowing beads represent the active initiator and monomer, while the reacting initiator and monomer are shown by pink and blue beads connected by a solid blue line. Unreacted monomers are depicted by the typical blue beads. (c) The hydrophobic surfaces S_1 and S_2 are depicted by green and red beads, and the yellow bead represents oil. For clarity, water beads are not shown in this or any forthcoming figures in this work. (d) The homogeneous structure $t = 0$ of water, oil, and JPs is illustrated.

3.3 Result and discussion

Polymer brush modification of MP surface.

In this section, we modify spherically shaped MPs by growing polymer brushes using surface-initiated ATRP, forming JPs. We consider three different initiator concentrations (1.0%, 2.5%, and 5.0%) to examine the chemical kinetics that affect the growth of the polymer brushes and to verify the simulation parameters. To analyze the polymer reaction kinetics, we calculate the monomer conversion, $Conv_M = [M]_r/[M]_0$, and $\ln([M]_0/[M]_u)$ as a function of brush growth time, t_{bg}. Here, $[M]_0$ refers to the initial monomer concentration, $[M]_r$ and $[M]_u$ refer to the reacted and unreacted monomer concentrations, respectively. Fig. 3.2(a) displays $Conv_M$ vs.

t_{bg} for different initiator concentrations up to $t_{bg} = 1.2 \times 10^3$ for $N_{MP} = 20$ MPs in the system. At these conditions, the monomer conversions are 8.6% for $c_i = 1.0\%$ (black curve), 11.2% for $c_i = 2.5\%$ (red curve), and 19.4% for $c_i = 5.0\%$ (green curve). The monomer conversion rate is faster for $c_i = 5.0\%$ compared to the other concentrations, indicating that higher initiator concentration promotes more efficient brush growth on the MP surface. It is essential to note that these plots depict the initial monomer conversion. However, $Conv_M \rightarrow 1.0$ is observed at much later times. For $c_i = 1.0\%$ (black curve) and 2.5% (red curve), a longer waiting time is required to achieve full monomer conversion. The inset of Fig. 3.2(a) demonstrates linear polymerization kinetics: $\ln([M]_0/[M]_u)$ vs. t_{bg} for various c_i values. However, the reaction rate kinetics deviate slightly from linearity at late times when $Conv_M \rightarrow 1.0$, which indicates pseudo-first-order kinetics (not shown here). Therefore, our model accurately captures the expected polymerization kinetics and the attributes of living radical polymerization.

To demonstrate how the length of grafted brush affects the emulsification of oil in water, we synthesize MP surfaces $(N_{MP} = 20)$ at different t_{bg} while maintaining a constant $c_i = 5.0\%$. In Fig. 3.2(b), the black, red, and green curves represent the increasing monomer conversion at t_{bg} of 1.2×10^3, 1.8×10^3, and 3.0×10^3, respectively. Within these time intervals, we observed $Conv_M$ to be approximately 19.4%, 29.2%, and 46.3% of the total monomer concentration $(\phi_M = 2.5 \times 10^{-1})$. The nearly linear relationship of $\ln([M]_0/[M]_u)$ with reaction time confirms the accurate replication of pseudo-first-order kinetics by the DPD polymerization scheme. Consequently, the resulting polymer brush-modified MPs are referred to as JPs. Moreover, these above choices of monomer conversion at $c_i = 5.0\%$ for the specified brush growth period are further used in Fig. 3.6 to demonstrate the impact of brush length variation grafted on JP surfaces on the oil-in-water emulsification.

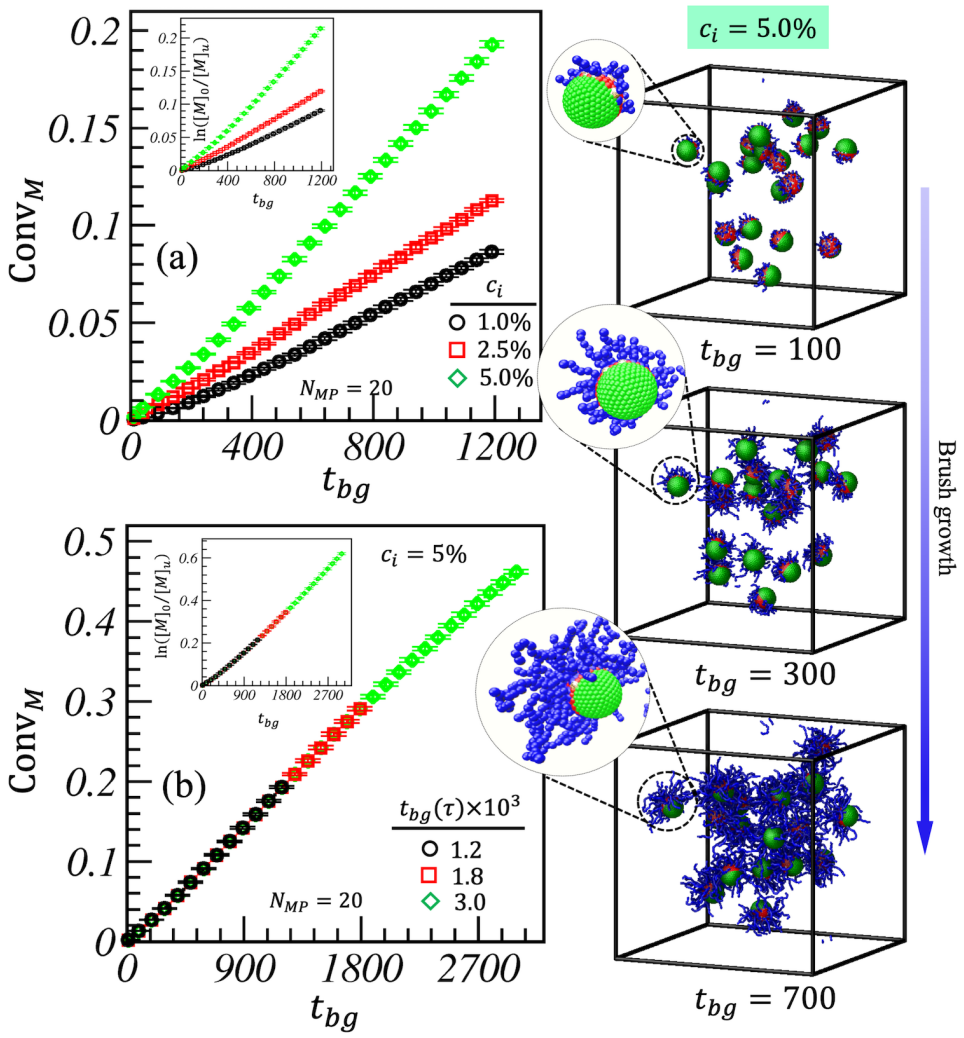

Fig. 3.2: (a) Monomer conversion ($Conv_M$) is shown for different initiator concentrations: $c_i = 1.0\%$ (in black), 2.5% (in red), and 5.0% (in green) of MP over brush growth time (t_{bg}). Within the system, there are 20 MPs. ATRP is done for $t_{bg} = 1.2 \times 10^3$. The rate kinetics are displayed in the inset as $\ln([M]_0/[M]_u)$ vs. t_{bg}. (b) Monomer conversion is displayed for various $t_{bg} = 1.2 \times 10^3$ (in black), 1.8×10^3 (in red), and 3.0×10^3 (in green) at a constant $c_i = 5.0\%$. The corresponding reaction rate kinetics are displayed in the inset. The polymer brush growth (in blue) on the S_2 surfaces (in red) over time is shown in the right panel. For better visibility, a zoomed image of a brush-modified JP is shown to enhance the clarity.

Kinetics of emulsion formation in the presence of JPs at $c_i = 1.0\%$.

This study examines a system consisting of 20 MPs embedded with an initiator concentration of 1% (equivalent to 5.3×10^{-4} initiators). The MPs were fabricated with polymer brushes up to a value time $t_{bg} = 2.6 \times 10^3$, resulting in JPs with $Conv_M$ of approximately 19.4% of N_M. This

corresponds to an average grafted brush length (degree of polymerization) of approximately $l_b \sim 91$ (in reduced DPD units). At the start of the emulsification process marked as $t = 0$, we introduced oil beads with a concentration of $\phi_o = 5.0 \times 10^{-2}$. The system's solvent (water) volume fraction is approximately $\phi_s = 8.4 \times 10^{-1}$. Oil segregation was observed at different times, specifically at $t = 5.0 \times 10^2$, 2.0×10^3, 8.0×10^3, and 2.6×10^4, to study the oil-in-water emulsion with brush-modified JPs, as depicted in Figs. 3.3(a-d). For clarity, solvent beads were omitted from the illustration. These images display oil emulsification in water, with oil beads gathering around the compatible S_1 surfaces of JPs staying away from the incompatible brushes (grafted at S_2 surfaces) localized at the oil-water interfaces.

The scaled correlation function, $C(r,t)$ vs. $r/R(t)$ is shown in Fig. 3.3(e) to describe the oil morphology illustrated in Figs. 3.3(a-d). The order parameter is calculated as explained in Sections 1.9 and 3.2.2. A slight deviation from the dynamic scaling is noticeable at $t = 2.0 \times 10^3$ (black). This behavior is commonly attributed to the significant difference in composition between the solvent and oil phases (off-critical composition) [197]. However, the scaling functions are well fitted and observed for later times, $t = 8.0 \times 10^3$ (red), 1.6×10^4 (green), and 2.6×10^4 (blue). This suggests the oil morphologies later fall under the same dynamical universality class. The unscaled correlation function for the same time intervals is also shown in the inset. It is apparent that the $C(r,t)$ vs. r data for later times, particularly at $t = 8.0 \times 10^3$ (in red) and beyond, are closely aligned. The 0.2 crossing of the correlation function determines the average domain size. Therefore, our results confirm the minimal change in the domain size, indicating the pinning effect in domain growth and stable oil-in-water emulsion formation. Also, note the discontinuity in $C(r,t)$ data as $r/R \to 0$, which is typically attributed to the formation of a rough/fuzzy oil morphology resulting from the wetting of JPs at the oil-water interface [41,195].

In this study, we examine the growth of the average domain size, $R(t)$ vs. t, on a log-log scale in Fig. 3.3(f) to demonstrate power-law growth for the morphology shown in Figs. 3.3(a-d). The

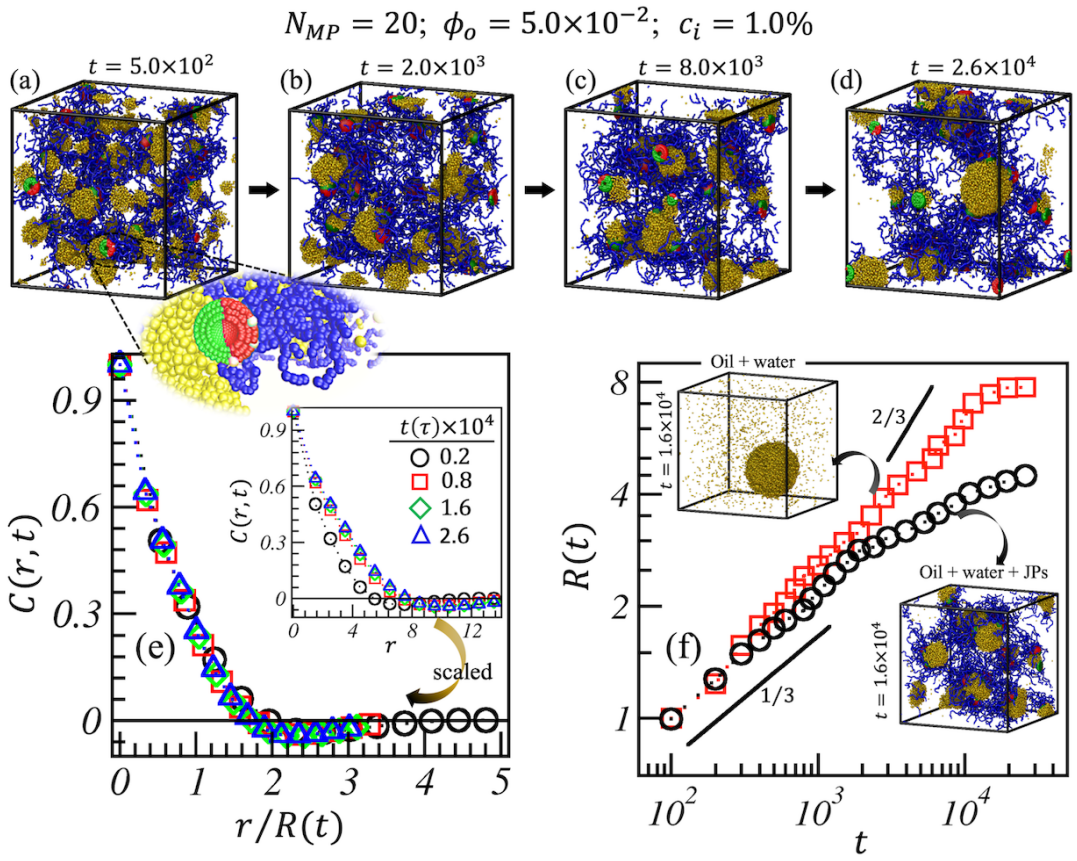

Fig. 3.3: Oil emulsion evolution through brush-modified JPs at different time t values: 5.0×10^2, 2.0×10^3, 8.0×10^3, and 2.6×10^4 are shown (a-d). The blue beads represent the polymer brushes. There is also a close-up picture of a JP molecule modified by a brush for better understanding. To ensure picture clarity, the water droplets are not shown. The volume fraction of oil is $\phi_0 = 5\times10^{-2}$. (e) The scaled $C(r,t)$ vs. $r/R(t)$ plots at $t = 2.0\times10^3$, 8.0×10^3, 1.6×10^4, and 2.6×10^4 are denoted by black, red, green, and blue symbols. The solid line guides the zero-crossing of $C(r,t)$. The inset shows the corresponding unscaled $C(r,t)$ vs. $r/R(t)$ plots. (f) Characteristics length scale, $R(t)$ vs. t for the evolution snapshots in panels (a–d) is shown in black symbols. The red curve exhibits the same for the pure oil and water mixture. Their corresponding late-time morphologies are shown in the inset. The solid lines with slope $1/3$ and $2/3$, representing growth exponents, are drawn for reference.

red curve represents the time variation of $R(t)$ for a composition of pure oil ($\phi_o = 5.0\times10^{-2}$) and water ($\phi_S = 8.1\times10^{-1}$) mixture [9,10]. The inset shows the corresponding morphology for $t = 1.6\times10^4$. It is important to note that in the DPD simulation of pure binary fluid segregation, the diffusive growth ($\phi \sim 1/3$) is transient. The system quickly transitions to hydrodynamic regimes with higher growth exponents [29]. The red curve in our study illustrates

this observation. The length scale deviates from diffusive growth and crosses over to the inertial hydrodynamic growth regime ($\phi \sim 2/3$) at late times. Ultimately, the length scale saturates beyond $t \approx 1.5 \times 10^4$. This behavior is attributed to the finite-size effect within the system (separate from the effect of JPs in emulsification) [9,10]. This behavior is characteristic of complete phase separation in pure binary fluids at late stages, where cluster size becomes comparable to the system size, resulting in the cessation of further system kinetics [9,10]. Based on this, simulating our system up to $t = 2.6 \times 10^4$ (in reduced DPD units) is adequate to observe the stability of emulsion formation at the time and length scales of our simulation

Further, in the presence of brush-modified JPs, $R(t)$ initially grows diffusively ($\phi \sim 1/3$) for a short time up to $t \approx 1.5 \times 10^3$ (shown in black). After that, it slows down significantly towards a much lower $R(t)$ value, moving towards the saturation regime. The corresponding morphology can be seen in the inset of Fig. 3.3(f). This contrasts with the red curve, which shows a much higher $R(t)$ value. The noticeable change in $R(t)$ can be attributed to the brush-modified JPs wetting the oil-solvent interface, which reduces interfacial tension and restricts the growth of oil clusters. This observation validates the stabilizing effect of oil emulsification with brush-modified JPs. It is important to note that prolonged stabilization of oil-water emulsions or similar complex systems can be quite challenging owing to the inherently dynamic nature of fluid phases [198–201]. Therefore, the coalescence of a few dispersed oil droplets over time cannot be disregarded, as it may affect the overall emulsion stability [198,199]. It is experimentally proven.

Effect of brush-modified JPs prepared at fixed monomer conversion on emulsification

We fabricate the MP's S_2 surface to make JPs by growing polymer brush for three different initiator concentrations: $c_i = 1.0\%, 2.5\%$, and 5.0%. The polymer brushes were allowed to grow until $t_{bg} = 2.6 \times 10^3$, 2.0×10^3, and 1.2×10^3 to achieve the same monomer conversion, $Conv_M \approx 19.45\% N_M$, respectively. The corresponding average grafted chain lengths (degree

of polymerization) are $l_b \approx 91, 35$, and 18, respectively. This means that, for each c_i, we maintained the same brush density within the system while the length of the grafted chains differed (l_b is longer for lower c_i and vice versa). However, the local brush density for an individual JP is higher for higher c_i.

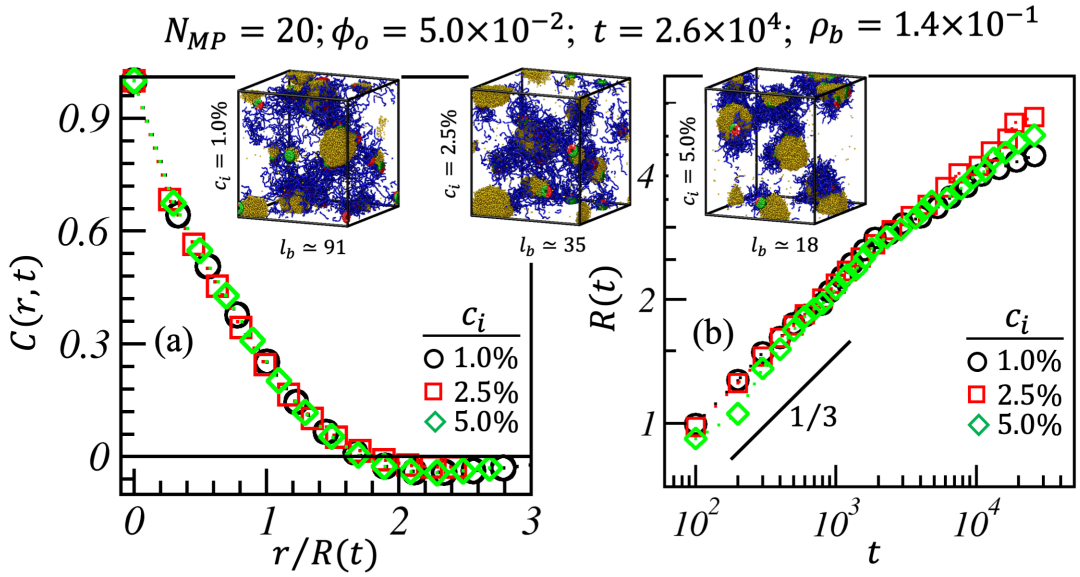

Fig. 3.4: (a) A comparison of $C(r,t)$ vs. $r/R(t)$ for different values of c_i (1.0% in black, 2.5% in red, and 5.0% in green) is shown for $t = 2.6 \times 10^4$. (b) The corresponding length scale, $R(t)$ vs. t is plotted on a log-log scale during the emulsification time. The insets show the corresponding morphologies of oil emulsion in the solvent by brush-modified JPs for a fixed $Conv_M \approx 19.45\% N_M$.

The inset figures in Fig. 3.4 display the different morphologies of the oil-in-water emulsion. They indicate the potential impact of polymer brush length on emulsion formation at a fixed polymer brush density. It is challenging to visually distinguish the effect of these JPs on the emulsion formation. Therefore, we use correlation functions and the temporal variation of the average domain size to characterize these emulsion morphologies in Fig. 3.4(a) and Fig. 3.4(b). In Fig. 3.4(a), we observe excellent data overlap of the scaled correlation functions ($C(r,t)$ vs. r/R), shown by black ($c_i = 1.0\%$), red ($c_i = 2.5\%$), and green ($c_i = 5.0\%$) curves at $t = 2.6 \times 10^4$. This suggests the statistical similarity of evolved morphologies, placing them within the same dynamical universality class. Moreover, a noticeable discontinuity in the $C(r,t)$

as $r/R \to 0$ indicates a fuzzier oil morphology resulting from the wetting of JPs at the oil-water interface. The time variation of the average domain size ($R(t)$ vs. t) is displayed in Fig. 3.4(b).

In the beginning, all three data sets show diffusive growth. Instead of transitioning to a higher growth rate for pure oil-water off-critical mixture, the domain growth significantly slows down, displaying a much lower growth rate than in diffusive growth (as shown by the solid black line with a $1/3$ slope). This confirms the formation of stabilizing emulsions for all c_i at later stages. Notably, a lower initiator concentration, $c_i = 1.0\%$, results in slightly slower domain growth and an early trend toward saturation at late times. This is because a lower c_i leads to a longer brush length when the monomer conversion is constant. Longer brushes appear to inhibit the clustering of oil more effectively than the other two cases, as brushes are incompatible with the oil beads. Additionally, we consider $c_i = 2.5\%$ ($l_b = 35$, red curve) and $c_i = 5.0\%$ ($l_b = 18$, green curve) for the late-time comparison. It can be inferred from these results that when there is not a substantial difference in brush length, the increased brush density observed at the JP surface for $= 5.0\%$ exerts a dominant influence over brush length, resulting in a slightly more efficient stabilization of emulsification.

Effect of local brush density on JPs with fixed brush length on emulsification

Here, we modified the S_2 surfaces of 20 MPs (fabricated MPs are JPs) for three initiator concentrations: $c_i = 1.0\%, 2.5\%$, and 5.0%. This will result in different grafted brush densities. The polymer brushes are allowed to grow up to $t_{bg} = 6.0 \times 10^2$, 1.0×10^3 , and 1.2×10^3 for the different c_i values, respectively. The corresponding monomer conversion for each case is approximately 3.8%, 9.7%, and 19.5% of N_M, leading to a grafted brush length of approximately 18 for each case. Consequently, the brush densities for the three cases are approximately $2.89 \times 10^{-2}, 7.26 \times 10^{-2}$, and 1.45×10^{-1}, respectively. Therefore, we maintain a uniform length of the grafted brushes within the system for each c_i, while the brush density increases with increasing c_i.

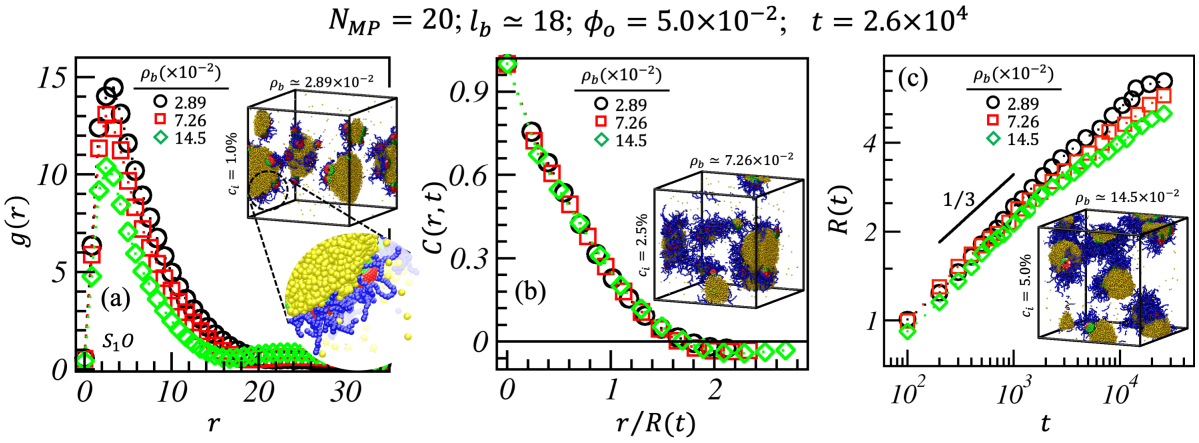

Fig. 3.5: (a) The graph shows the radial distribution function, $g(r)$ vs. r, for oil around the S_1 surface. A close-up view of a brush-modified JP molecule is depicted for improved clarity. (b) Comparison of a scaling function, $C(r,t)$ vs. $r/R(t)$, for three different brush densities represented by different symbols at $t = 2.6 \times 10^4$. (c) The graph illustrates the time variation of length scale, $R(t)$, for three different brush densities. The inset of Figure (a), (b), and (c) respectively, shows the corresponding oil emulsion morphologies by brush-modified JPs with the same brush length $l_b \approx 18$ but different brush densities, $\rho_b \approx 2.89 \times 10^{-2}, 7.26 \times 10^{-2}$, and 14.5×10^{-2}.

The emulsion formation is characterized by comparing the radial distribution function (RDF), $g(r) = \rho_{io}/\rho_o$, of oil beads around the S_1 surface of JP, corresponding to the evolution patterns displayed in Fig. 3.5 at different densities. Here, $\rho_{io} = n_{io}(r)/V_{shell}$ is the local oil density around any i^{th} reference surface bead. The parameter, $n_{io}(r)$, is the number of oil beads in a shell of width $dr = \sqrt{(|dx|^2 + |dy|^2 + |dz|^2)}$ and volume V_{shell} at a distance r from the i^{th} reference bead; $\rho_o = N_o/V$ is the average number density of oil beads in the system where N_o and V denote the total oil beads and volume of the system. We investigate the impact of brush-modified JPs with varied brush density, while the brush length is fixed at $l_b \simeq 18$, on the emulsification process of oil ($\phi_o = 5.0 \times 10^{-2}$) within a solvent ($\phi_s \simeq 8.4 \times 10^{-1}$). The images in Figs. 3.5(a-c) show the resultant oil emulsion morphologies at $t = 2.6 \times 10^4$. The corresponding radial distribution function (RDF) of oil beads around the S_1 surface for $\rho_b = 2.89 \times 1^0 - 2, 7.26 \times 10^{-2}$, and 1.45×10^{-1} is illustrated in Fig. 3.5(a) using black, red, and green symbols, respectively. The black curve indicates a higher peak height, suggesting

that more oil beads cluster around the S_1 surface for $\rho_b = 2.89 \times 10^{-2}$. A lower brush density creates a porous region at the S_2 surface, causing more oil beads to be found near the S_2 surface due to favorable interactions between the oil beads and S_2 surface (excluding polymer brushes). This explains the higher RDF peak around S_1 for $\rho_b = 2.89 \times 10^{-2}$. As the brush density increases, the porosity within the brush region decreases, resulting in a reduced RDF peak.

The graph in Fig. 3.5(b) shows the scaled correlation function ($C(r,t)$ vs.r/R) curves for $\rho_b = 2.89 \times 10^{-2}$ (in black), 7.26×10^{-2} (in red), and 1.45×10^{-1} (in green) at $t = 2.6 \times 10^4$. The perfect overlap of the data indicates that the evolved morphologies are statistically similar, confirming they belong to the same dynamical universality class. In Fig. 3.5(c), the time variation of the average domain size ($R(t)$ vs. t) is displayed. In the early stages, all three datasets show diffusive growth. However, the domain growth significantly slows down compared to the typical phase segregation observed in off-critical binary fluid mixtures, as shown by the red curve in Fig. 3.3(f). This observation validates the stabilization of emulsification over time. It is worth noting that emulsification tends to stabilize further with higher brush density, as indicated by the green curve. This enhanced stabilization is attributed to the increased wetting of the oil-water interface with JPs possessing higher brush density. In addition, at the lowest brush density, the average domain size experiences a sudden increase in its value at $t \approx 1.42 \times 10^4$, which is attributed to the merging of two or more larger oil clusters. Similar phenomena are also observed in experiments, not shown here. Particles modified with higher macro-initiators are found to produce a larger hydrophilic lobe, thereby strongly adsorbing at the oil/water interface. This reduces their interfacial tension and prolongs the emulsion stability.

Effect of the grafted brush length on JP surface on oil emulsification

In this study, we examine the impact of different lengths of JP brush on the emulsification of oil $\phi_o = 1.0 \times 10^{-1}$ in water. We consider $N_{MP} = 20$ MPs with $c_i = 5.0\%$ initiators, and

approximately $\phi_M \simeq 2.5 \times 10^{-1}$ monomers in the solvent. The surface-grafted polymer brushes are grown at different times $t_{bg} = 0, 1.2 \times 10^3, 1.8 \times 10^3$, and 3.0×10^3. This resulted in brush lengths of $l_b \approx 0$, 24, 37, and 60 (in reduced DPD units).

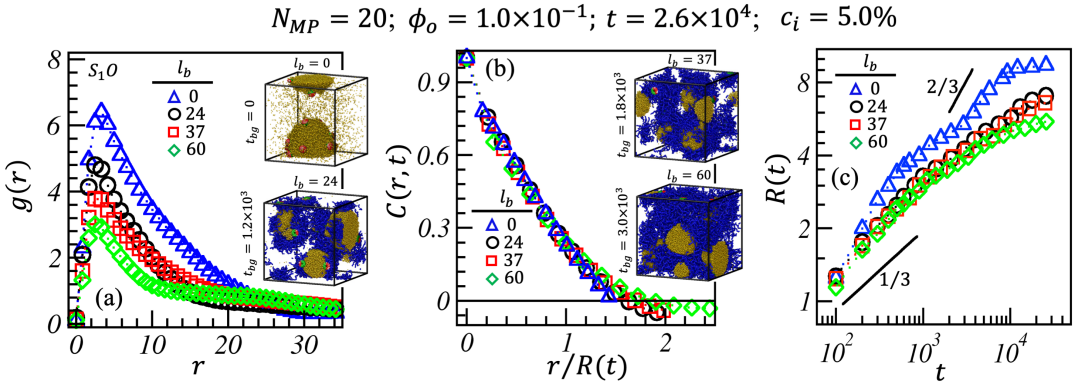

Fig. 3.6: The graph in (a) shows the radial distribution function, $g(r)$ vs. r, for oil around the S_1 surface with different symbols indicating various brush lengths. In (b), there is a comparison of scaling functions ($C(r,t)$ vs. r and $R(t)$) at $t = 2.6 \times 10^4$. (c) presents the characteristic length scale ($R(t)$ vs. t) on a logarithmic scale. Additionally, the inset of Figures (a) and (b) shows the corresponding evolution morphologies of oil emulsion by brush-modified JPs for brush lengths $l_b \approx 0$, 24 and $l_b \approx 37$, 60, respectively.

The oil morphologies at different brush lengths are shown in the inset of Figs. 3.6(a-b) at the emulsification time, $t = 2.6 \times 10^4$. To understand or characterize the morphology of the oil, we first plot $g(r)$ vs. r for oil beads around the S_1 surface in Fig. 3.6(a) for the different brush lengths shown. The blue, black, red, and green lines represent the $g(r)$ data for $l_b \approx 0$, 24, 37, and 60, respectively. We noticed that the peaks in the RDF graphs became less distinct and wider as the brush length increased. This suggests that more oil beads formed clusters across the S_1 surfaces when $l_b = 0$. It is important to note that when $t_{bg} = 0$ ($l_b = 0$), both of the MP surfaces are able to attract oil beads (only the initiators on the S_2 surfaces repel water). This means the oil beads surround a larger part of the MPs, limiting their movement to the interface between the oil and the solvent. This leads to the easier transport of oil and water across the interface, forming larger clusters of oil and water. With the growth of solvent-compatible polymer brushes on S_2 surfaces, MPs transform into JPs. Thus, with increasing brush length l_b of 24, 37, and 60, modified JPs diffuse more promptly at the oil-solvent interface, leading to

improved arrangements across it. This results in decreased interfacial tension [41] and reduced oil clustering across the S_1 surface. It is important to note that estimating interfacial tension in a phase-separating system is only feasible for well-separated flat interfaces [202,203]. As a result, we have not estimated this quantity in our simulation. However, we have compared experimental data for interfacial tension, showing that the interfacial tension is minimal in the presence of modified JPs compared to unmodified JPs (MPs) and pure fluid mixtures. Furthermore, the interfacial tension progressively decreases with increased macroinitiator content in JPs (meaning that BP25 JPs are strongly adsorbing at the oil/water interface compared to the BP10 JPs). This indirectly suggests that the brush density plays a role in stabilizing the o/w-based Pickering emulsion.

We have plotted the scaled correlation function, $C(r,t)$ vs. $r/R(t)$, in Fig. 3.6(b) for $l_b \approx 0$ (in blue), 24 (in black), 37 (in red), and 60 (in green) at $t = 2.6 \times 10^4$. A noticeable deviation from the dynamical scaling is observed for $l_b = 0$ (blue curve) compared to the other scaling functions at $l_b \neq 0$. This suggests that the clustering of oil beads at $l_b = 0$ is statistically distinct from the clustering observed in the presence of JPs ($l_b \neq 0$). However, there is considerable overlap in the data for scaling functions at $l_b \neq 0$, indicating that they belong to the same dynamical universality class. The temporal evolution of the characteristic domain size, $R(t)$ vs. t, is displayed on a log-log scale in Fig. 3.6(c), corresponding to the scaling functions shown in Fig. 3.6(b). A solid black line with a slope $\phi = 1/3$ represents the expected diffusive growth for a limited time window. The black, red, and green curves show early diffusive growth, which noticeably slows down and tends toward saturation. The smallest average domain size is observed in the green curve, which transitions to the saturation phase earlier than the black and red curves. This suggests a more stable emulsification for longer brushes, i.e., $l_b = 60$. The blue curve ($l_b = 0$) shows a clear deviation from early diffusive growth to a much higher growth exponent, as expected for highly off-critical phase-separating binary fluids. Thus, for $l_b = 0$, the transportation of oil and water beads across the interface is hardly constrained by

JPs as they are not well settled at the oil-water interface and predominantly remain in the oil phase. Later, we observed a crossover to the inertial hydrodynamic growth ($\phi \sim 2/3$) regime, confirming that stable emulsification does not occur at $l_b = 0$.

Effect of number and size of JPs on oil emulsification

Now we emphasize the impact of JP's size on oil $\phi_O = 1.0 \times 10^{-1}$ emulsification in a solvent, where the volume fraction of MP is fixed at $\phi_{MP} = 5.7 \times 10^{-2}$. As the number of MPs increases, their size decreases and vice versa, keeping the overall number of initiators at the MP's surfaces fixed at $c_i = 5.0\%$. We used $N_{MP} = 20, 40$, and 80 MPs to prepare brush-grafted JPs. The hydrophilic brushes at the initiator-embedded S_2 surfaces were allowed to grow for $t_{bg} = 3.0 \times 10^3$ in the presence of monomers ($\phi_M = 2.5 \times 10^{-1}$) in a compatible solvent ($\phi_S \simeq 6.0 \times 10^{-1}$). The average brush length, $l_b \simeq 66$ for each size of JP.

We examined the different oil morphologies in the inset of Fig. 3.7 for $N_{MP} = 20$, 40, and 80 at $t = 2.6 \times 10^4$. To describe these structures, we plotted the average length scale, $R(t)$ vs. t, on a logarithmic scale. The early diffusive growth exponent is represented by a solid black line, with a value of $\phi \sim 1/3$ for a short period. As expected, having $N_{MP} = 80$ JPs (smaller in size) increases the wetting of the oil-solvent interface due to their smaller size, leading to faster diffusion. This results in a more significant reduction in interfacial tension compared to $N_{MP} = 20$ and 40, consequently restricting the domain growth. Therefore, the growth in $R(t)$ for $N_{MP} = 80$ is significantly reduced and tends toward the saturation phase much earlier (green curve), indicating more stable emulsification compared to $N_{MP} = 40$ and 20 (red and black curves). Furthermore, akin to previous instances, a much-extended waiting period in this scenario may eventually result in the coalescence of oil particles.

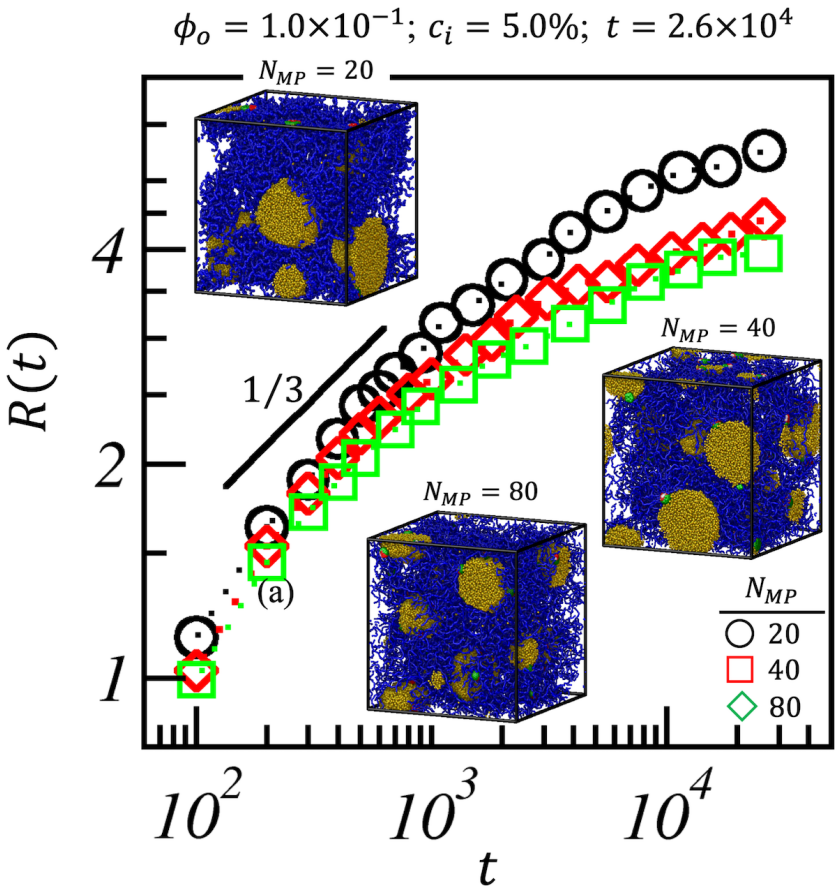

Fig. 3.7: The graph displays the length scales, $R(t)$ vs. t, for the oil emulsion at different numbers (and sizes) of JPs. Specifically, N_{MP} is equal to 20 (black curve), 40 (red curve), and 80 (green curve) for a fixed brush length, l_b, which is approximately 66. The inset shows the corresponding evolutionary morphologies of oil-in-water emulsion at $t = 2.6 \times 10^4$.

3.4 Conclusion

Our research focused on investigating the formation of stable oil-in-water Pickering emulsions using polymer brush-modified JPs, employing a combined numerical and experimental approach. Through in-depth DPD simulation, we analyzed the chemical and physical processes at the microscopic level. Our simulation model captured the first-order chemical kinetics of living free radical polymerization, demonstrating linear polymer growth over time through reaction rate kinetics, thus justifying our simulation parameter selection.

In the broader context, brush-modified JPs significantly stabilized the oil-in-water emulsion, regardless of size, number, grafting brush density, and brush length, compared to unmodified JPs. However, among brush-modified JPs, the stabilization of oil/water emulsification varied under different conditions. When comparing JPs with different initiator concentrations but at a constant monomer conversion, we maintained a constant overall brush density. Thus, JPs with a lower initiator concentration exhibited longer brush lengths, supporting more stabilized emulsion formation by effectively restricting oil clustering compared to shorter chains. Similarly, considering JPs with different initiator concentrations but by suitably varying the monomer conversion, we fixed the length of grafted polymer brushes, leading to surface modification with different local grafting brush densities. Higher initiator concentration implied enhanced grafting density and vice versa. In this scenario, we observed a more stable emulsification in the presence of JPs with high brush density. At a constant initiator concentration (fixed local surface brush density), varying the length of polymer brushes resulted in a more stable emulsion with longer brushes. Additionally, we demonstrated the impact of adjusting the size of modified JPs while maintaining equal lengths of grafted chains. A reduction in JP size, while keeping the total MP density constant, increased the number of JPs. Smaller-sized JPs, higher in number, notably enhanced interface wetting, leading to the early slowing down of cluster growth and, consequently, a more stable emulsification.

Our experimental findings indicated that the emulsions remained stable for a week, regardless of the size and brush density of the particles. However, particles with higher brush density (those with 25% macro initiator content) appeared to provide extended stability to the emulsion, aligning with the simulation results described above. Nevertheless, experiments showed no impact on emulsion stability by changing the size of the brush-modified JPs within the specified conditions. This dissimilarity between experimental and simulation outcomes can be attributed to the constant volume fraction of JPs in the simulation. Overall, our experimental findings

support and align well with the simulation results, providing a comprehensive understanding of the factors influencing stable emulsion formation.